# Multiplex Coatings

Hosson, Jeff T.M. De; Pei, Yutao

*Published in:*
Encyclopedia of Tribology



*Publication date:*
2013

960 meshes for a line contact EHL problem was 4 h on a scientific computer in 1985 (Lubrecht, et al. 1986), while it was less than 1 s (excluding the time for edit and link) on a personal computer in 2009, see the entry entitled ► Multi-Grid Method in this Encyclopedia.

## References


A. Brandt, A.A. Lubrecht, Multilevel matrix multiplication and fast solution of integral equations. J. Comput. Phys. **90**, 348–370 (1990)

B.J. Hamrock, D. Dowson, Isothermal elastohydrodynamic lubrication of point contacts, part III – fully flooded results. ASME J. Lubr. Technol. **99**, 264–276 (1977)

Y.Z. Hu, D. Zhu, A full numerical solution to the mixed lubrication in point contacts. ASME J. Tribol. **122**, 1–9 (2000)

M. Kaneta et al., Effects of elastic moduli of contact surfaces in elastohydrodynamic lubrication. ASME J. Tribol. **114**, 75–80 (1992)

X. Liu et al., Non-Newtonian thermal analyses of point EHL contacts using the Eyring model. ASME J. Tribol. **127**, 70–81 (2005)

A.A. Lubrecht et al., Multigrid, an alternative method for calculating film thickness and pressure profiles in elastohydrodynamically lubricated line contacts. ASME J. Tribol. **108**, 551–556 (1986)

S. Qu et al., Theoretical investigation on the dimple occurrence in the thermal EHL of simple sliding steel-glass circular contacts. Tribol. Int. **33**, 59–65 (2000)

C.H. Venner et al., Advanced multilevel solution of the EHL line contact problem. ASME J. Tribol. **112**, 426–431 (1990)

C.H. Venner, Multilevel solution of the EHL line and point contact problems, Ph.D. thesis, The University of Twente, Enschede, 1991

C.H. Venner et al., Film thickness modulations in starved elastohydrodynamically lubricated contacts induced by time-varying lubricant supply. ASME J. Tribol. **130**, 041501 (2008)

P. Yang et al., On the theory of thermal elastohydrodynamic lubrication at high slide-roll ratios – line contact solution. ASME J. Tribol. **123**, 36–41 (2001)

P. Yang et al., Influence of two-sided surface waviness on the EHL behavior of rolling/sliding point contacts under thermal and non-Newtonian conditions. ASME J. Tribol. **130**, 041502 (2008)


# Multiplex Coatings


M. De Jeff T. Hosson, Yutao Pei
Department of Applied Physics, Materials Innovation Institute and Zernike Institute for Advanced Materials, University of Groningen, Groningen, AG, The Netherlands


## Definition

The tribological performance of nanocomposite diamond-like carbon (DLC) coatings and the breakdown of the Coulomb friction law in nanocomposite materials are discussed here. Physical arguments are provided to explain the dependence of friction on sliding velocity, in the context of self-lubrication and influence of water vapor adsorption from the testing environment. From a structural design viewpoint, nanocomposite coatings exhibit an optimized combination of functionalities when a nanoparticle becomes approximately the same size as the separation.

## Scientific Fundamentals

### Introduction

Many laws in phenomenological materials physics are based on the concept that a constant driving force will lead to a response that is stable in time. In fact, the entire framework of solid state mechanics, founded by Isaac Newton himself, is based on this principle. In the field of materials science, this concept was believed to be true also. For example, a constant load will lead to a particular deformation response everywhere and at any time in the material; a constant frictional load will generate a constant sliding velocity for two surfaces in contact, and so on. Nevertheless, in recent times it has been demonstrated convincingly that in many situations such a concept does not apply. Typical examples being the jerky motion of dislocations when deforming a metal (De Hosson et al. 1983) or the jerky (stick-slip) motion of surfaces in relative motion (Kerssemakers and De Hosson 1998). Since the time of Leonardo da Vinci, who was arguably the first engineer to study friction in detail, stick-slip phenomena at interacting surfaces have become an important branch of modern materials science and engineering. Due to the complexity of friction processes combining individual physical events between sliding surfaces, it is still, however, a challenge to understand the precise mechanisms of stick-slip friction on a micrometer scale. Indeed friction between two surfaces in relative motion is a complex phenomenon that involves phonon dissipation, bond breaking and formation, strain-induced structural transformation and local surface reconstruction, and adhesion. From a physics point of view, it is determined by short- and long-range interactions between the surfaces. However, the underpinning mechanism of friction and the upscaling from atomic phenomena to microscopic effects are still not understood. The classical friction laws were discovered by da Vinci and Guillaume Amontons, respectively, and were summarized much later by Charles Augustin Coulomb, who also contributed the third friction law. The three laws of friction describe that the friction force to resist sliding at an interface is (1) proportional to the normal force between the surfaces, (2) independent of the apparent contact area, and (3) independent of the sliding velocity. In this contribution it is shown that

nanocomposite diamond-like carbon (DLC) materials may show a breakdown of the Coulomb friction law.

## Friction of Nanocomposite DLC Coatings

A panoply of testing techniques has been developed to examine the tribological performance of PVD coatings. While the actual applications of DLC coatings in the automotive industry are often under lubricated contacts, tribological tests without lubricants and in ambient air or controlled atmospheres allow the investigation of the physical mechanisms that affect self-lubrication effects. The results of these tests do not always guarantee that a coating will be successful in a particular application, but they assist in determining the mode of wear of different coating materials in the stage of coating design and development. The well-defined loading conditions employed in laboratory tests may be different from those of real applications where lubricant and even abrasive particles are often present. Indeed, abrasive wear resistance is of paramount importance in many tribological applications, and so is the interaction of the oil and oil additives with the coating material. The temperature of the coated components in the contact is an important factor influencing the tribological behavior of the coatings. The thermal stability of the substrate material is also important in this sense in that the substrate needs to maintain its mechanical properties to properly support the coating in the contact.

DLC-based coatings may exhibit low friction, which has been attributed to the possible formation of a transfer layer on the surface of the uncoated counterpart. Recent research has paid some attention to the effects of transfer films on friction behavior, but their importance is still rather overlooked. The friction behavior of hydrogenated and hydrogen-free DLCs differs in the formation mechanism of transfer films within the contact. The former makes the contact between two similar hydrophobic DLC surfaces and in the latter a graphitic layer acts as solid lubricant. The influence of environment on the friction of DLC-based materials is a topic of controversy and remains under continuous debate. Contradictory reports can be found of the effects of adsorbed gases on the friction coefficient. For example, Zaïdi et al. observed that the steady-state coefficient of friction (CoF) of graphite fell as the partial pressure of oxygen gas increased or as the sliding velocity decreased (Zaïdi et al. 1990). In contrast, Heimberg et al. noted that adsorbed gases appeared to increase the CoF of hydrogenated DLC films (Heimberg et al. 2001). Obviously, the surface characteristics of materials play a crucial role in the tribological performance. The influence of the adsorption of $N_2$ gas by DLC material during dry sliding experiments, causing a variation of friction coefficients with sliding speed and with time, has been explained by some authors through the use of the Elovich equation. The same equation can also describe our experimental results if only the adsorption of water vapor is considered. The friction behavior of TiC/DLC nanocomposite coatings is more complicated compared with pure DLCs. It has been shown that the presence of TiC nanocrystallites influences the formation of transfer layer, and in the case where the DLC matrix cannot efficiently shield TiC particles in the transfer films, as in the case of nanocomposite coatings with a large volumetric fraction of TiC nanocrystallites, TiC nanoparticles may hamper the formation of the transfer layer.

It is possible to deposit hydrogenated *nc*-TiC/*a*-C:H coatings by a closed-field unbalanced magnetron sputtering in an argon/acetylene atmosphere, using a coating system, configured with two Cr targets and two Ti targets, each pair being vertically opposed. The detailed set-up of the coating system has been documented elsewhere (Pei et al. 2005). The acetylene flow rate and substrate voltage bias were varied each in the range of 80–125 sccm (standard cubic centimeters per minute) and 0–150 V, respectively, to obtain different C/Ti ratios and nanostructures in the coatings. The coatings are named in such a way that the numbers preceding the character "V" indicate the substrate bias (in volts), and those following the acetylene flow rate (in sccm). Representative graphs of friction coefficient versus running laps are shown in Fig. 1a, where three different kinds of friction behavior of the nanocomposite coatings are recognized (Tay et al. 2000). The coating 0 V110 exhibits a nearly constant CoF and the coating 100 V80 shows rather large fluctuations in the friction coefficient curve. The mean CoF of the coatings 0 V110 and 100 V80 is above 0.2 (i.e., much higher than that of the rest four coatings). The other four coatings show not only a low steady-state CoF, but also a quick drop in the CoF from an initially high value of about 0.2 at the beginning of sliding until the transition point where the steady state is reached. This behavior is attributed to the gradual formation of a transfer film on the counterpart surface during the early stage of a tribotest, which makes the contact in between two basically similar hydrophobic DLC surfaces that contribute to self-lubrication. Against different counterparts (i.e., sapphire, alumina, and bearing steel balls), only slight differences in the friction coefficient are observed on the coatings with self-lubrication. This may imply that the interfacial sliding actually takes place between the transfer films on the ball and the surface of

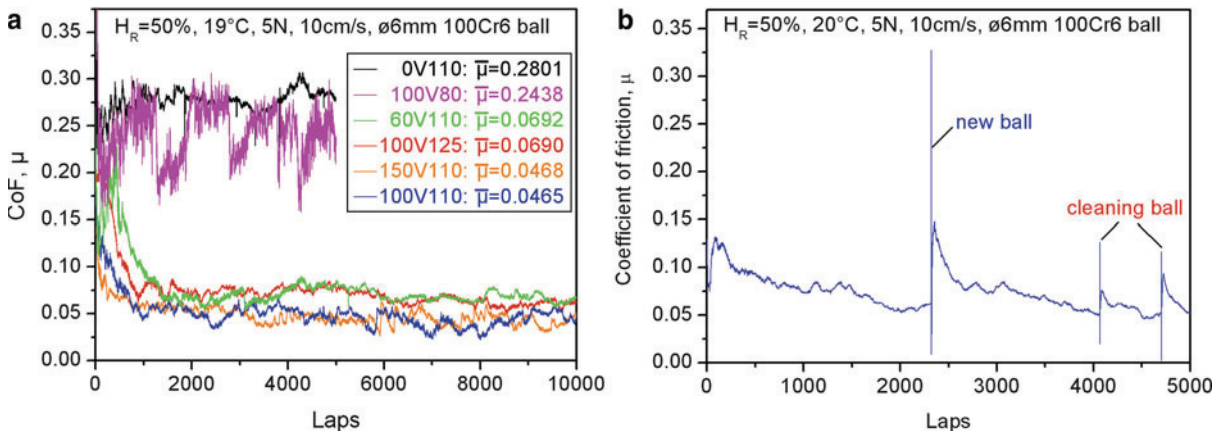


**Multiplex Coatings, Fig. 1** (**a**) Graph of coefficient of friction versus number of laps of the coatings under dry sliding against 100Cr6 steel ball and (**b**) self-lubricating effect of coating 100 V110

the coating, rather than sliding between the surfaces of the counterpart and the coating.

To prove that the self-lubrication is induced by the formation of transfer films, experiments were done in such a way that a fresh surface area of the ball was placed on the same wear track after the stationary state was reached (Fig. 1b). The friction coefficient immediately jumped to a value that characterizes the friction between the fresh steel surface and the coating. Again, the friction coefficient dropped down quickly as the transfer films gradually covered the ball surface. Further experiments have been carried out to demonstrate the effect of cleaning the contact area of the ball by rinsing with ethanol and drying with dry $N_2$. Cleaning resulted in small peaks in the graph of friction coefficient followed by another quick drop in friction. However, the friction coefficient at the maximum of these peaks is lower than that when a fresh surface of the ball was brought into contact with the wear track, which may be possibly attributed to partially adhered films that could not be cleaned completely.

## Influence of Sliding Velocity and Humidity

Figure 2 shows graphs of CoF versus laps for coatings 100 V80 and 100 V110, tested at different sliding velocities. The CoF graphs of coating 100 V80 in Fig. 2a are nearly horizontal curves with large fluctuations, and the mean values of CoF at different velocities are almost the same (i.e., 0.218, 0.216, and 0.227 at different sliding velocities of 10, 30, and 50 cm/s, respectively). Apparently, the coating 100 V80 without a self-lubricating effect exhibits a CoF that is independent of the sliding velocity. In other words, the Coulomb friction law holds in this case. In contrast, the CoF of coating 100 V110 drops quickly from an initial high value of about 0.2 at the beginning of sliding to a very low value of CoF ($<0.05$) at the steady state, which is attributed to self-lubricating effects. A strong dependence of the steady state CoF on the sliding velocity is observed such that the faster the sliding velocity, the smaller the CoF (Fig. 2b). The steady state CoF of coating 100 V110 at sliding velocities of 10, 30, and 50 cm/s is 0.047, 0.030, and 0.013, respectively. It is clear that the Coulomb friction law is no longer valid when self-lubrication occurs, leading to jerky-type behavior.

The effects of relative humidity on friction are demonstrated in Fig. 3a. In general, the CoF of coating 100 V110 decreases with decreasing humidity. However, peaks have been recorded in the CoF curves when the relative humidity is equal to 25% or lower and they occur more often in dry air if the sliding velocity stays constant. This implies that the sliding velocity used is close to the limit in dry air and also raises the steady-state CoF slightly. These CoF peaks are attributed to the frequent breakdown of the transfer film as described above. Such a decrease of CoF with humidity has also been observed for coating 100 V125, where only a couple of peaks in the CoF curve occurred in dry air so that a monotonic decrease of CoF with decreasing humidity was recorded. By comparing the frequency of the CoF peaks in dry air between the coatings 100 V110 and 100 V125, it should be pointed out that the critical sliding velocity is also affected by the volumetric fraction of *a*-C:H matrix: the wider the TiC particle separation in the matrix, the higher the critical velocity will be.

The dynamic response of CoF to humidity and the corresponding change in the transfer film thickness are shown in Fig. 3b. Three levels of relative humidity

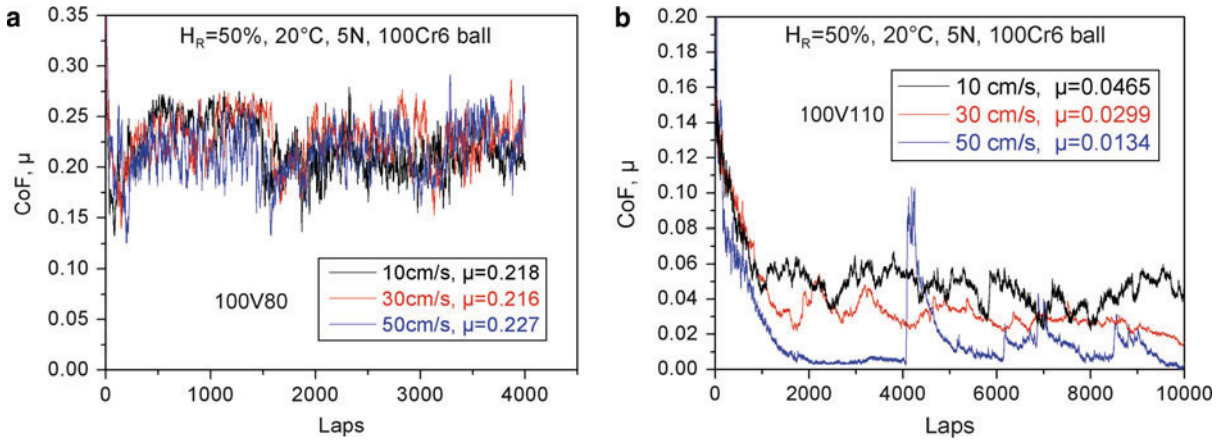


**Multiplex Coatings, Fig. 2** Influence of sliding velocity on the coefficient of friction of the coatings: (**a**) 100 V80 and (**b**) 100 V110 under dry sliding against 100Cr6 steel ball

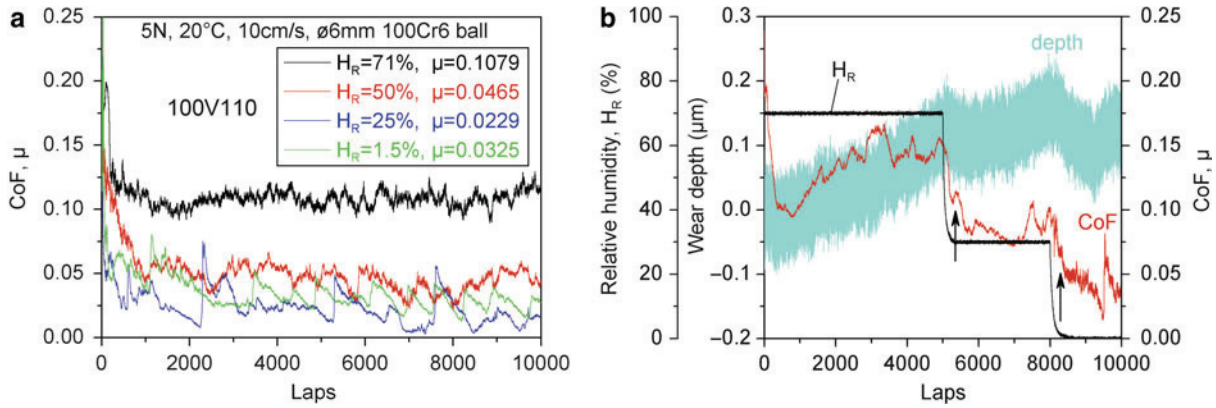


**Multiplex Coatings, Fig. 3** (**a**) Effects of relative humidity on the CoF of the coating 100 V110 and (**b**) CoF dynamic response to humidity of coating 100 V125

(i.e., 70%, 30%, and 0%) were employed in a single-run tribotest run, where the transitions from high to low humidity were quickly realized by purging dry air into the testing chamber of the tribometer. It is interesting to note the change of CoF over the humidity transition periods. The CoF drops immediately once the humidity falls. Although the drop of CoF continues after the transition periods, there is a small step in the CoF decay corresponding to the end of the humidity drop, as marked by arrows in Fig. 3b, after which the slope of the CoF drop is further reduced. This points to different mechanisms involved in the reduction of friction. Thickening of the transfer film starts immediately after the humidity drops and lasts much longer than the transition periods, indicated by the segments of depth curve with a negative slope as shown in Fig. 3b. Apparently, this thickening contributes to the whole course of the CoF drop. On the other hand, the thickness and coverage of adsorbed water molecular layer on the fresh transfer film and wear track are determined by the relative humidity and decrease as humidity lowers during the transition periods. It is understood that energy dissipation to the water molecular layer will accordingly decrease in the transition periods until a lower level is reached at lower humidity. This transition period is reflected in the first steep decline of CoF before the steps.

## Adsorption and Friction

A lower humidity and a higher sliding velocity have similar effects on the frictional behavior of the self-lubricating

coatings, that is, they result in the formation of thinner transfer films that provide a lower friction coefficient. It is expected that both dependencies originate from the same microscopical mechanism – the influence of the water vapor condensation on the rheology of the transfer layer. The surface coverage of the adsorbed gas on a solid surface as a function of time ($t$) can be successfully described empirically using the so-called Elovich equation (Elovich and Zhabrova 1939):

$$\frac{dq}{dt} = Ae^{-\alpha q} \tag{1}$$

which can be integrated as

$$q = \frac{1}{\alpha}\ln(\alpha A) + \frac{1}{\alpha}\ln(t + \frac{\beta}{\alpha A}) \tag{2}$$

where α is a constant associated with the number of available adsorption sites over the surface and $A$ is a constant related to the flux of adsorbing gas, which was found to be proportional to its partial pressure in certain cases of non-dissociative adsorption. β is determined by integration of (2) from the initial condition ($t_i$,$q_i$) to the situation of ($t$,$q$), that is,

$$e^{\alpha q_i} - A\alpha t_i = e^{\alpha q} - A\alpha t = \beta \tag{3}$$

When at the onset $q_i$ and $t_i$ are taken to be equal to zero, β is equal to unity. In a ball-on-disk tribo-test, each time the ball counterpart passes a point on the circular wear track, it "wipes" a contact area. Thereafter, the contact area is re-exposed to gases in the environment for new adsorption. The exposure time ($t$) between two successive wipes is inversely proportional to the sliding velocity ($v$):

$$t = \frac{2\pi \cdot r}{v} \tag{4}$$

where $r$ is the radius of the wear track.

The Elovich equation was employed successfully to interpret the dependency of the friction coefficient of DLC coatings on the exposure time to a dry $N_2$ atmosphere (Heimberg et al. 2001). It is clear that the parameter governing the frictional behavior of the nanocomposite coatings is the relative humidity, which is directly proportional to the partial pressure of water vapor in the testing atmosphere. The fractional coverage of water vapor on the coating surface during the ball-on-disk test can be estimated as a function of the relative humidity and the sliding velocity, respectively (see Fig. 4). The experimental results indicate that the adsorption of water vapor is responsible for the frictional behavior, supported by the fact that the coefficient of friction of the coatings changes in a consistent trend with the fractional coverage of water vapor.

## Influence of Temperature on Tribological Performance

In order to reveal the thermal resistance of the coatings, the variation of their hardness and elastic modulus was monitored by nanoindentation experiments after annealing them for 1 h at various temperatures in air. The DLC coatings are thermally stable up to 250°C but start to soften at 300°C. The softening of annealed coatings becomes pronounced above 350°C. In contrast, it is known that the mechanical properties of bearing steels (e.g., 100Cr6) degrade at a temperature of about 190°C. Figure 5 demonstrates the tribological performances of the

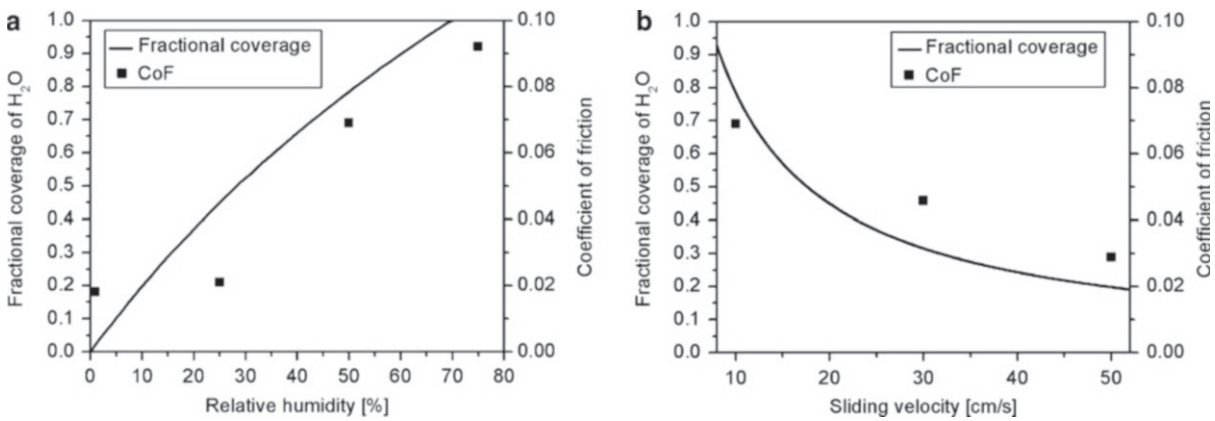


**Multiplex Coatings, Fig. 4** Comparison between the CoF of coatings and the fractional coverage of water vapor on wear tracks calculated according to (2): (**a**) influence of relative humidity at sliding velocity of 10 cm/s and (**b**) effect of sliding velocity at 50% relative humidity

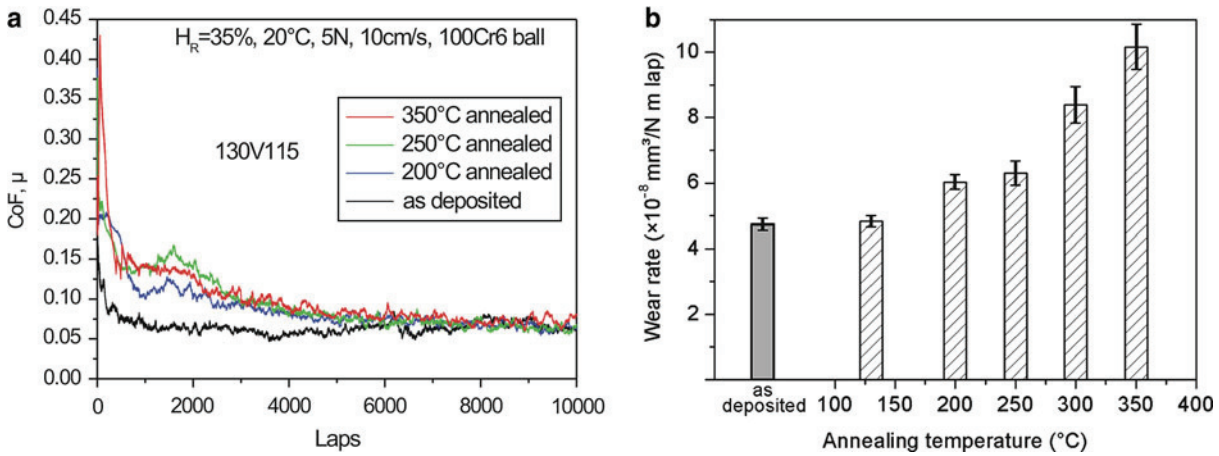


**Multiplex Coatings, Fig. 5** Influence of annealing temperature on the tribological properties of coating 130 V115: (**a**) coefficient of friction (CoF) and (**b**) wear rate, tested at room temperature and 35% relative humidity, 5 N normal load and 10 cm/s sliding velocity against 100Cr6 ball

as-deposited and annealed coatings, respectively, as tested with ball-on-disk dry sliding against ø6 mm 100Cr6 balls under 5 N normal load and 10 cm/s sliding speed.

The as-deposited coatings show the typical self-lubricating behavior observed. That is to say, the CoF drops from an initially high value of about 0.2 at the beginning of sliding to a low steady-state CoF of about 0.06–0.08, after a transition period during which transfer films gradually form over the surface of the ball counterpart. The wear rate of the annealed coatings remains quite stable up to the annealing temperature of 250°C and increases significantly when annealed at temperatures above 300°C. In addition, the coatings annealed at higher temperatures exhibit a higher CoF at the onset of a tribotest and need longer to reach the low steady state CoF. For instance, the peak CoF at the beginning of sliding for the coatings annealed at 350°C is twice as high compared with the values measured for coatings annealed below 250°C. In other words, annealing at higher temperatures deteriorates the self-lubrication effect.

Auger depth profiles of the oxygen concentration in the as-deposited and annealed DLC coating is shown in Fig. 6 and reveals that oxidation of TiC/DLC coatings during 1 h annealing in air is negligibly small up to the annealing temperature of 250°C. A substantial increase in oxygen content has been detected after annealing at 300°C. However, the diffusion depth of oxygen is limited to about 100 nm in the annealed coating. Annealing for a longer time or at higher temperatures will increase further the oxygen content as well as the diffusion depth in the coatings, which may result in heavier degradation of the annealed coatings. This oxidation behavior of a thin surface layer explains the higher initial CoF and the longer transition period needed to reach the steady state CoF for the coatings annealed at higher temperatures. Indeed, a CoF value as high as 0.28 was observed for the DLC coating that contains 16 at.% oxygen.

Ball-on-disk tribotests were performed starting at room temperature and gradually increasing the temperature during the test. The ultra-low friction regime of TiC/DLC coatings may maintain up to 200°C, as shown in Fig. 7, where the CoF (∼0.01) is lower than the steady state CoF of the coating tested at room temperature. The friction coefficient gradually increases to a value of 0.1 as the temperature rises above 200°C. Thereafter, the coating suddenly fails at about 230°C with a sliding life shorter than 3,000 laps (revolutions), indicated by a peak in the friction trace up to a value of about 0.6. The latter is a typical CoF value for dry sliding between metal-to-metal contacts. This indicates that coating delamination is the failure mechanism, as confirmed by SEM observations in Fig. 7b.

The two different levels of CoF before abrupt failure of the coating deserve special comments. At the early stage of a test the CoF drops to a very low value of about 0.01 as the sample temperature rises rapidly towards 100°C. This phenomenon is attributed to the gradual desorption of water molecules from the sliding surfaces with increasing temperature, whose effect is equivalent to that of decreasing the humidity level of the atmosphere. When the sample temperature is above 200°C, the coating surface oxidizes locally at the hot spots on sliding contact where

the peak temperature may be well above 350°C. This leads to an increase in oxygen content in the top atomic layers of the coatings and consequently a significant increase in CoF, close to the CoF value of the annealed coatings. In addition, the 100Cr6 ball counterpart starts to soften at such high temperatures, which may destroy the transfer films and lead to adhesive wear due to the higher friction coefficient. Ultimately it results in delamination of the coating, as observed in Fig. 8b.

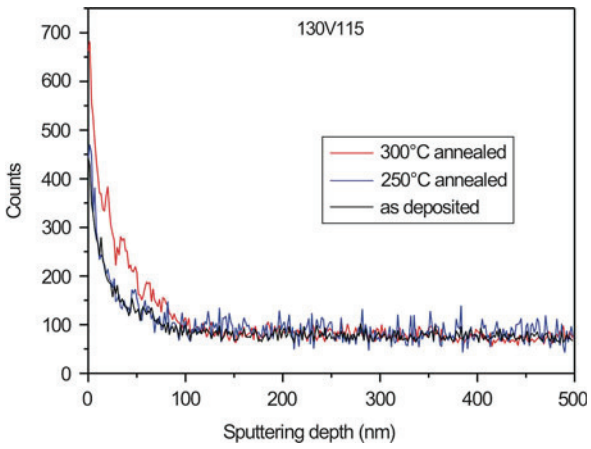


**Multiplex Coatings, Fig. 6** Auger depth-profiling of oxygen element in the coating 130 V115 after annealing at different temperatures in comparison with that of the as-deposited coating

It is known from the literature that DLC-based coatings are stable under annealing in air up to temperatures of at least 250 °C (Tay et al. 2000). Nevertheless, it has been shown that a degradation mechanism is present during the elevated temperature tribotests that limit their use to lower temperatures. The introduction of alloying elements in H-free DLC coatings reduces their hardness and their wear resistance, but decreases considerably the sliding friction coefficient at ambient temperature. Chemical alloying is therefore an efficient approach to vary the properties of DLC coatings for different applications. Nevertheless, care should be taken when selecting DLC coatings for applications at elevated temperatures. Indeed, in the higher temperature range all coatings provide lower friction coefficients than typically observed at ambient temperature. Pure DLC coatings are able to provide a sliding friction coefficient below 0.1 during sliding at high temperature up to 285°C, while the presence of Ti and Si alloying elements may decrease the maximum operating temperature of the coatings to 160°C.

## Influence of Nanostructure and New Developments

In nanocomposite coatings composed of hard nanograins and a compliant matrix, two different designs have been recently put into practice in thin film applications, namely superhard and supertough nanocomposite coatings (Cavaleiro and De Hosson 2006). The concept of superhard nanocomposite coatings is based on the suppression of dislocation operation by using 3–5 nm small

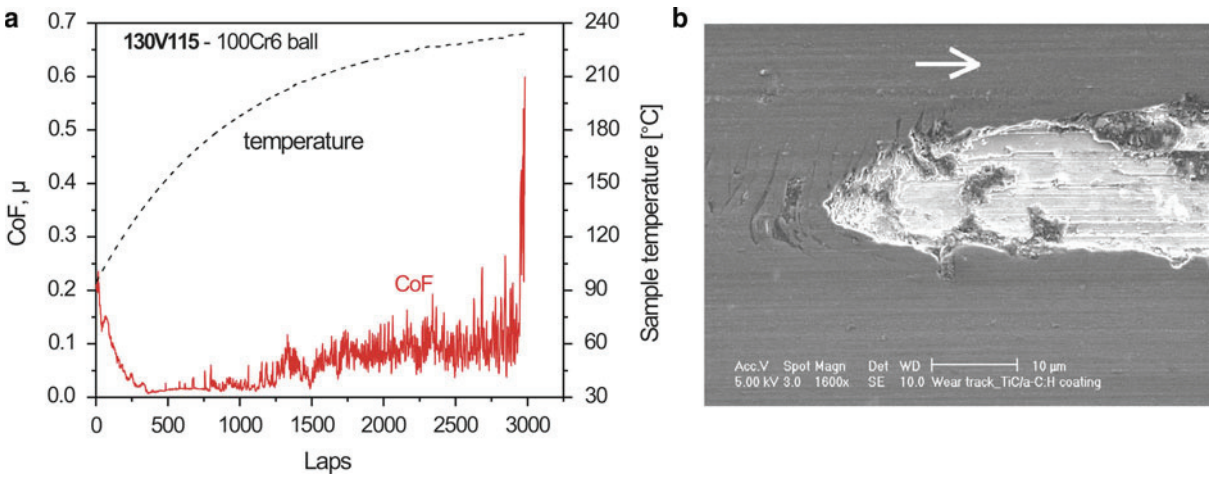


**Multiplex Coatings, Fig. 7** Elevated temperature tribo-testing results of the coatings: (**a**) 130 V115 tested in air of 50 % relative humidity, 5 N normal load, 10 cm/s sliding velocity. (**b**) SEM micrograph of the middle part of the wear track on the coating 130 V115 showing a damaged spot where the coating delaminated during the elevated-temperature tribo-test. An *arrow* indicates the moving direction of the ball counterpart

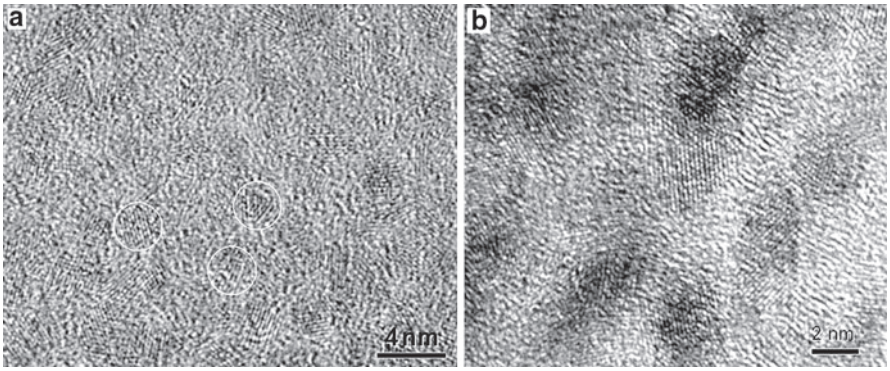


**Multiplex Coatings, Fig. 8** HR-XTRM micrographs showing (**a**) homogeneously distributed TiC nanocrystallites in TiC/a-C:H nanocomposite coating 100 V110 and (**b**) aligned TiC nanocrystallites separated by amorphous carbon matrix sub-layers of tunable thickness in a TiC/a-C nanocomposite coating (the multilayers are tilted about 60° to the bottom border of the micrograph)

grains and inducing grain incoherence strains with <1 nm thin matrix for grain separation. On the other hand, nanocomposite coatings generate a high density of interphase interfaces that assist in crack deflection and termination of crack propagation. The introduction of amorphous matrix may facilitate grain sliding that releases the strain energy stored. Based on these toughening mechanisms, the concept of supertough nanocomposite coatings has been proposed. For super toughness, a coating structure consisting of 10–20 nm nanocrystalline grains separated by 2–10 nm amorphous matrix has been suggested (Voevodin and Zabinski 2003). However, such a combination of large nanograins with a wide matrix separation is not favored regarding atomic migration during deposition. Magnetron sputtering with a negative substrate bias not higher than 150 V and without intentional substrate heating is less likely to generate atomic displacement over a distance of several nanometers through surface diffusion or subsurface migration. Therefore, many nanograins with sizes smaller than 10–20 nm are formed in the amorphous matrix with separations that are determined by the elemental concentration. In recent work on TiC/a-C:H nanocomposite coatings (Tay et al. 2000), the minimum size of TiC nanocrystallites observed is 2 nm. The particle size does not increase until the matrix separation diminishes with increasing Ti content to a certain limit, due to the competition between grain nucleation and grain growth. Based on these observations, a toughening mechanism of delocalizing cracks has been proposed. That is to say, keeping the suppression of crack nucleation in an amorphous matrix, the introduction of nanoparticles may spread the localization of cracks into a delocalized state. The ductility and therefore the toughness will be enhanced provided the particle size becomes of approximately the same size as the separation.

As is clear from the aforementioned results the size and separation of TiC nanocrystallites in the DLC-based nanocomposite coatings are crucial for tribo-functionality. Self-lubricating effects have been only observed on the TiC/*a*-C:H nanocomposite coatings once the separation of the nanocrystallites in the *a*-C:H matrix is sufficiently wide, that is to say, a mean separation distance close to the size of the TiC nanoparticles. In fact nanocrystalline TiC (*nc*-TiC) particles may serve as a promoter for surface graphitization of the a-C:H matrix that leads to ultra-low friction. Surface graphitization of the *a*-C:H matrix is boosted due to the high localized shear stresses applied by the exposed *nc*-TiC in the transfer films (nano-scaled asperities). On the other hand, these TiC nanocrystallites also scratch the coating surface and facilitate wear. As a result, there is a trade-off between CoF and wear rate towards the low volume fraction of *nc*-TiC. It is thus understandable that the nanocomposite coatings exhibit even smaller CoFs than those of pure DLC coatings (typically 0.1 ∼ 0.15 under comparable conditions of loading and counterpart), where such hard and sharp nanoscaled TiC asperities are missing. The interesting point here is that various combinations of CoF and $W_R$ can be selected for different applications according to whether a high wear resistance or a low friction is the principal objective.

A new development is highlighted in Fig. 8, showing that a nanocomposite coating can be designed of homogeneously distributed TiC nanocrystallites or aligned TiC nanoparticles. To manipulate size and separation of TiC nanocrystallites, a possible approach is to tailor a

multilayered structure into a nanocomposite coating, such that the nanocrystallite containing sub-layers are separated by the matrix sub-layers of desired thickness via composition fluctuation during deposition. Through such an integrated multilayer-composite structure, the size and separation of TiC nanoparticles can be controlled independently (Fig. 5b), which was not possible in a homogeneous nanocomposite coating. It turned out that the multilayered nanocomposite coating exhibits essential enhancement in fracture toughness and it is hardly possible to induce radial cracks via nanoindentation with a cube-corner diamond indenter even if the indenter has penetrated through the entire coating thickness. In particular, its tribological performance is also superior and comparable with the advanced TiC/a-C:H nanocomposite coatings (Pei et al. 2006). Further detailed characterization of the nanostructure and properties of TiC/a-C nanocomposite coating are published elsewhere (Pei et al. 2008; Chen et al. 2009). TiC/hydrogenated DLC coatings are stable after annealing in air up to a temperature of at least 250°C. No variation of their mechanical properties or appreciable oxidation was observed. Its wear resistance also remained unchanged up to this temperature. Nevertheless, tribological tests at high temperature resulted in failure of the self-lubrication mechanism and subsequent coating failure at temperatures around 200°C.

## Key Applications

From an industrial point of view, during the 1980s the applications of the Me-DLC coatings were very limited. The company Balzers tried to commercialize the Me-DLC coatings and in particular the W-C:H, but no large production volumes were achieved. It was not until approximately 1994–1995 that the first large-scale industrial production of the Me-DLC coating was started by the company of Robert Bosch GmbH. The application concerned parts for the first generation of high-pressure diesel fuel injection systems for engines and the coating used was a W-C:H coating. The coating is used on critical components in the injection system to avoid scuffing and abrasive/adhesive wear due to the very high injection pressures used in, for example, common rail diesel fuel injection systems. PVD and PA-CVD coatings are widely used today in the diesel fuel injection systems and have become a necessity for survival of critical components when the injection pressure is rapidly approaching 2,000 bar. No diesel fuel injection system would today survive without PVD and PA-CVD coatings.

It is expected that the demand for tribological coatings will grow for industrial applications in the near future. There are several factors contributing to this development. One important factor is the rapid development of engine technology in the automotive industry over the last years. Today, the demand for components in an engine leads to higher precision in the tolerances for machining. The growing precision for components is not only demanded when the engine is brand new, but also over the lifetime of the engine. One of the main reasons for this is the need to control all parameters in the combustion accurately to lower fuel consumption and emissions from the engines. In general, components today are also expected to have a longer lifetime with less maintenance intervals. This has significant impact on the wear situation of many components in the engine. Another important driving force for coating engine components with PVD coatings is the increasing power density components are exposed to in modern engines, and here especially the diesel engine plays an important role. The introduction of the common rail diesel fuel injection system in 1997 has led to an ever-increasing need to protect components by tribological coatings, not only in the diesel fuel injection system itself, but also in many other areas in the engine. The reason for this development is the increased injection pressures of diesel that results not only in cleaner combustion and less fuel consumption but also in higher power and torque of the engine.

The injection pressure of today's generation of common rail is approximately 1,800–2,000 bars and the next generation that will be introduced in a couple of years' time will exceed 2,000 bars. At these extremely high pressures, many components in the diesel fuel injection system cannot survive without protective DLC-type coatings to prevent, for example, abrasive wear and seizure of the components. The increased power and torque also creates a significantly higher power density in many power train components, since it is not permissible to design bigger or heavier components in modern engines due to space and weight saving. On the contrary, many components are today both more highly loaded and at the same time smaller and lighter. Critical areas include valve train components like tappets and rocker arms, piston rings and pins in the piston assembly, and journal bearings in the crankshaft area.

To tackle these problems, automotive engine design engineers try to use primarily conventional surface engineering technologies like higher quality steels, better performing heat treatments, and improved surface finish by the use of better grinding and polishing techniques. The reason for this is mainly cost and caution regarding introduction of new technology in mass production. Only when conventional technologies no longer work for the function of a component is alternative surface engineering

considered. However, there are a few exceptions to the above discussion. In some industrial applications, there has been an opportunity to replace the steel material of the original part with cheaper steel with a PVD coating deposited on top. The end result has been a component that performs better and is cheaper than the original part. This is, of course, the ideal situation for applying a PVD coating.

The results presented here show that it is possible to tailor coating properties to accommodate the need for different industrial applications. For example, in an industrial application like roller bearings it is important that the coating is low stressed and has an excellent fatigue resistance to being able to survive in the application and provide the expected extension in lifetime compared with uncoated roller bearings. The results indicate that a relatively soft and multilayered Me-DLC coating would be suitable for this type of application. The combination of low coefficient of friction with moderate hardness and stress in combination with an excellent fatigue resistance indicates that it could perform well. Another example is the industrial application of coatings on diesel fuel injection parts. The plunger used in the pump for building up the very high injection pressure (up to 2,000 bars in the latest generation of common rail systems) is typically coated. The requirements for this application are to reduce scuffing and seizure of the plunger to the very tight bore. Much abrasive wear is normally also present, since the fuel might be contaminated with particles. The typical coating used to solve these problems in the application is nanocomposite DLC based.

Chemical effects, in particular, should be considered if the influence of the atmosphere on the coefficient of friction must be explained. For a-C:H a low humidity atmosphere is the preferred condition for low friction. The H-terminated surfaces of both counterparts ensure their contact occurs under low adhesion, so that the transfer layer will be kept at the optimal thickness. The presence of humidity influences the surface properties of the counterparts, increasing their adhesion. Under these conditions the thickness of the transfer layer will vary under sliding contact, with subsequent increase of friction, which will increase wear, modifying the transfer layer thickness and leading to an unstable situation that will finally lead to high-friction sliding. For H-free a-C the situation is different, in that in this case the transfer layer formation is "dynamic," with graphite plates continuously transferring between coating and ball, because of the low shear rate along the basal planes of graphite. The ease of mutual sliding of the graphite basal planes can be improved with the presence of intercalated water molecules, giving a very different behavior as compared with a-C:H. Also in this case, when the transfer layer thickness has reached an optimum thickness there will be a stable situation, as the corresponding low friction will ensure no further modifications of its thickness will occur. In this case sliding in vacuum or inert atmosphere leads to an unstable high-friction state. Under vacuum sliding, the $p_z$ orbitals of each graphite atom will be dangling on the surface unsaturated, which will increase the adhesion between two such surfaces enormously, leading to high friction and wear and no possibility for transfer layer formation. Chemical effects are probably the reason why lamellar, low-shear strength materials such as $Ti_3SiC_2$ do not exhibit low friction following the formation of a transfer layer (El-Raghy et al. 2000), which is in contrast with the classical theory of low friction, which states that a low shear-strength material on top of a hard substrate is the desired low-friction configuration. To further support the framework presented here, the behavior of polymers such as HDPE (high-density polyethylene) and PTFE (polytetrafluoroethylene) sliding against glass can be mentioned (Hutchings 1992). These polymers form a transfer layer on the hard counterpart, but their initial coefficients of friction remain around 0.2–0.3, while the transfer layers are micrometers thick. As the sliding progresses the transfer layers become much thinner, and only then coefficients of friction as low as 0.05 are measured (for PTFE).

The following mechanism may be proposed to explain the jerky-type frictional behavior of the nanocomposite DLC coatings. The transfer film and the wear debris accumulated in front of the wear scar of the ball counterpart actually carry the contact load; their rheology is of prime importance in lowering the friction. When this nanosized debris is (in dry air) not covered by water molecules, they may be brought into (and easily sheared at) the sliding interfaces with a very weak interaction between themselves as well as between the surface of the wear track. However, at high sliding velocity the flow of debris into the sliding contacts may be interrupted due to the collapse of accumulated debris in front of the wear scar. Such collapses lead to the jerky-type behavior due to the frequent breakdown of transfer films and correspondingly to the peaks of CoF beyond the critical sliding velocity. At faster sliding velocity and/or lower level of humidity the films become thinner and looser and therefore they easily break. Collapses of the accumulated debris are expected to be more damaging to the thinner transfer films seen at higher sliding velocities. Condensation of water molecules collected from the surface of the wear track may change the nature of transfer films in humid air. It is well known that

adsorbed gases, especially water vapor, increase the rate of densification of particulate materials, for instance in the wear debris accumulated here. Therefore denser and thicker transfer films are formed at higher humidity and at lower velocity. One can conclude that it requires more energy mechanical work to slide and smear such a film than a loosely compacted and grainy one between the sliding surfaces.

## Acknowledgments

The authors acknowledge financial support from the Materials Innovation Institute–the Netherlands and the Foundation for Fundamental Research on Matter (FOM-Utrecht).

## References

A. Cavaleiro, J.T.M. De Hosson, *Nanostructured Coatings* (Springer, New York, 2006)

C.Q. Chen, Y.T. Pei, K.P. Shaha, J.T.M. De Hosson, J. Appl. Phys. **105**, 114314 (2009)

J.T.M. De Hosson, O. Kanert, A.W. Sleeswijk, in *Dislocations in Solids*, ed. by F.R.N. Nabarro (North-Holland, Amsterdam, 1983), pp. 441–534

S.Y. Elovich, G.M. Zhabrova, Zh. Fiz. Khim **13**, 1761 (1939)

T. El-Raghy, P. Blau, M.W. Barsoum, Wear **238**, 125 (2000)

J.A. Heimberg, K.J. Wahl, I.L. Singer, A. Erdemir, Appl. Phys. Lett. **78**, 2449 (2001)

I.M. Hutchings, *Tribology: Friction and Wear of Engineering Materials* (Edward Arnold, London, 1992). Co-published by CRC Press, Boca Raton, FL, USA

J.W.J. Kerssemakers, J.T.M. De Hosson, J. Appl. Phys. **83**, 3444–3445 (1998)

Y.T. Pei, D. Galvan, J.T.M. De Hosson, Acta Mater. **53**, 4505 (2005)

Y.T. Pei, P. Huizenga, D. Galvan, J.T.M. De Hosson, J. Appl. Phys. **100**, 114309 (2006)

Y.T. Pei, C.Q. Chen, K. Shaha, J.T.M. De Hosson, J. Bradley, S. Voronin, M. Cada, Acta Acta Materialia **56**, 696–709 (2008)

B.K. Tay, D. Sheeja, S.P. Lau, X. Shi, B.C. Seet, Y.C. Yeo, Surf. Coat. Technol. **130**, 248 (2000)

A.A. Voevodin, J.S. Zabinski, Thin Solid Films **370**, 223 (2003)

H. Zaïdi, D. Paulmier, J. Lepage, Appl. Surf. Sci. **44**, 221 (1990)

# Multi-Row Bearings

Xiaolan Ai
Timken Technology Center, The Timken Company, Canton, OH, USA

## Synonyms

Double-row bearings; Four-row bearings; Heavy-duty bearings; Multi-row self-aligning bearings; Package bearings

## Definition

Multi-row bearings are bearing assemblies with two or more rows of rolling elements arranged between raceways. Typical examples of multi-row bearings are spherical ball bearings, spherical roller bearings, and package bearings.

## Scientific Fundamentals

For the purpose of increasing load capacity, bearings are constructed with two or more rows of rolling elements. Two-row configurations are also constructed for self-retaining, for preloading, for bi-directional axial load carrying, or for reduction of internal friction losses. The following sections outline commercially available multi-row bearings.

### Double-Row Ball Bearing

Figure 1 shows a double-row deep-groove ball bearing. Both the inner and outer rings have two grooved raceways, one for each row of balls. The center distance of the two grooves on the inner ring is essentially the same as the center distance of the grooves on the outer ring. The bearing has two separate retainers for retaining two rows of balls, respectively. This bearing has greater radial load-carrying capacity than the single-row types. Load sharing is determined by the geometrical accuracy of the grooves. Double-row ball bearings perform similarly to single-row ball bearings.

The spacing between the centers of the two grooves on one ring can be controlled with respect to another ring to reduce the bearing axial clearance or to preload the bearing. This type of bearing is often classified as the double-row angular-contact ball bearing. When spacing between groove centers on the outer ring is greater than that of the inner ring, the bearing is referred to as the rigid type; when spacing between groove centers on the outer ring is smaller than that of the inner ring, the bearing is referred to as the non-rigid type. Double-row angular-contact ball bearings can carry thrust load in either direction or combined radial and thrust loads. Bearings of the rigid type are capable of handling moment load effectively. The bearings perform is essentially the same as duplex pairs of single-row angular-contact ball bearings.

### Self-Aligning Double-Row Ball Bearing

Figure 2 shows a double-row self-aligning ball bearing. It contains an outer race ring having an outer raceway, an inner race ring having two grooved inner raceways, two rows of balls, and two separate cages each retaining a row of balls. The outer raceway of this bearing is a portion of a sphere. Thus balls on the inner raceways are internally aligned to accommodate any misalignment, free from any